Automated Coarse-to-fine Segmentation of Thoracic Duct using Anatomy Priors and Topology-guided Curved Planar Reformation

Puyang Wang[1,2†], Panwen Hu[3†], Jiali Liu[*4†], Hang Yu[3], Xianghua Ye[5], Jinliang Zhang[6], Hui Li[6], Li Yang[6], Le Lu[1], Dakai Jin[1‡], and Feng-Ming (Spring) Kong[4‡]

[1] DAMO Academy, Alibaba Group
[2] Hupan Lab, 310023, Hangzhou, China
[3] The Chinese University of Hong Kong, Shenzhen
[4] The University of Hong Kong
[5] Zhejiang University
[6] The University of Hong Kong, Shenzhen Hospital
pauliwang411@gmail.com; liujiali1995@hotmail.com

Abstract. Recent studies have emphasized the importance of protecting thoracic duct during radiation therapy (RT), as dose distributions in thoracic duct may be associated with the development radiation-induced lymphopenia. Because of its thin/slim size, curved geometry and extremely poor (intensity) contrast of thoracic duct, manual delineation of thoracic duct in RT planning CT is time-consuming and with large inter-observer variations. In this work, we aim to automatically and accurately segment thoracic duct in RT planning CT, as the first attempt to tackle this clinically critical yet under-studied task. A two-stage coarse-to-fine segmentation approach is proposed. At the first stage, we automatically segment six chest organs and combine these organ predictions with the input planning CT to better infer and localize the thoracic duct. Given the coarse initial segmentation from first stage, we subsequently extract the topology-corrected centerline of initial thoracic duct segmentation at stage two where curved planar reformation (CPR) is applied to transform the planning CT into a new 3D volume representation that provides a spatially smoother reformation of thoracic duct in its elongated medial axis direction. Thus the CPR-transformed CT is employed as input to the second stage deep segmentation network, and the output segmentation mask is transformed back to the original image space, as the final segmentation. We evaluate our approach on 117 lung cancer patients with RT planning CT scans. Our approach significantly outperforms a strong baseline model based on nnUNet, by reducing 57% relative Hausdorff distance error (from 49.9mm to 21.2mm) and improving 1.8% absolute Jaccard Index.

Keywords: Thoracic Duct Segmentation, Radiation Therapy, Centerline Extraction, Curved Planar Reformation

---

[*] Corresponding author. [†] Equal contribution. [‡] Co-senior author
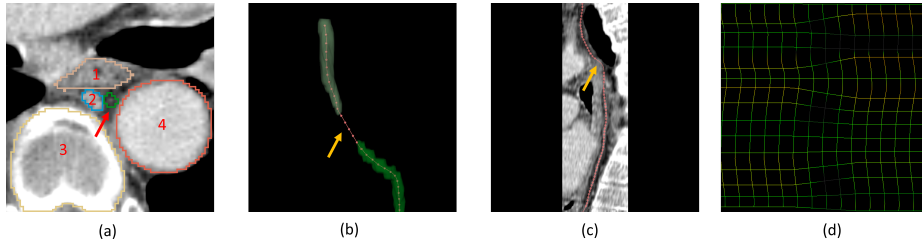
Fig. 1: (a) Thoracic duct indicated by red arrow (1: esophagus, 2: azygos vein, 3: spine, 4: aorta). (b) Segmentation breakage produced (indicated by yellow arrow) using the state-of-the-art segmentation method nnUNet [5] and the result of our topology-corrected centerline extraction. (c) CPR of CT scan based on extracted centerline. (d) CPR displayed in grid transform.

1 Introduction

Thoracic cancer is a significant public health challenge in the United States, with breast, lung, and esophageal cancers accounting for over 540,000 confirmed patient cases in 2022 alone [18]. Out of these patient poputations, approximately $50 \sim 60\%$ will receive radiation therapy (RT) as part of their treatment procedure [22]. While radiation is an effective treatment option for thoracic cancer, it also can cause severe toxic effects, e.g., radiation-induced lymphopenia (RIL), which is a condition that radiation dosage damages circulating immune cells and significantly impairs tumor control and patient survival [2, 20]. Several factors, such as mean lung dose, mean heart dose, and the effective dose to circulating immune cells (EDIC), are associated with the development of RIL [10, 19, 24]. Recent studies have showed the importance of protecting the thoracic duct during RT [15]. Thus it becomes essential for the accurate delineation of thoracic duct to minimize the risk of RIL in RT planning.

Thoracic duct, as the main collecting vessel of the lymphatic system, is a continuous tubular structure with a mean diameter of 2-3mm in the axial slices, and a mean intensity attenuation value of 15.3 HU (ranging between 4.5 to 38 HU) in CT scans that is slightly lower than that of arteries and veins [13, 16]. It is very challenging for accurate thoracic duct delineation due to its slim and curved 3D structure and the extremely poor contrast with surrounding adipose tissue in CT scans (see Fig.1 (a, b) for an illustration). Moreover, the low spatial resolution of RT planning CT may not adequately capture intricate details of the thoracic duct because the planning CT scans typically have the slice thickness between 3 and 5 mm with the pixel spacing of $1 \sim 1.2$mm in axial plane. The imaging quality can become even worse for some medical institutions when the planning CT is an average intensity projection CT generated from respiratory four-dimensional (4D-CT) scanning. All these factors compound the difficulty of manual delineation of thoracic duct, making it time-consuming with large inter-observer variability. This could ultimately lead to sub-optimal RT planning and produce potential radiation toxicity.

Recent advancements in deep learning have shown great promise in automated segmentation of organs at risk (OARs) and tumors in various body parts [1, 3, 4, 6–8, 23, 26]. UaNet adopts a segmentation-by-detection strategy to achieve 28 head & neck OAR segmentation [21], while SOARS [25] achieves a comprehensive of 42 head & neck OAR segmentation using stratified learning and neural architecture search [3, 25]. RTP-Net [17] develops a cascade coarse-to-fine segmentation scheme with organ size adaptive module and attention mechanisms for organ boundaries to segment 67 whole-body OARs. For thoracic OARs, a DeepStationing model has segmented 22 chest anatomical structures to support the mediastinal lymph node station segmentation [4], where high accuracy is achieved for OARs such as lungs, heart, esophagus and spinal cord. These studies demonstrate the capability of deep learning models to improve the OAR segmentation accuracy, consistency and reproducibility to benefit the RT planning in clinical practice. Nevertheless, none of the previous work have tackled thoracic duct segmentation. To address this challenging task, important anatomic knowledge and clinical insights can be leveraged. 1) Anatomy of thoracic duct is closely related to several key organs, e.g., near the level of the fifth thoracic vertebra, thoracic duct passes through the space between esophagus and spine. Physicians often utilize these reference organs to locate the spatial regions that thoracic duct may appear. 2) Considering that the relative low spatial resolution of planning CT, physicians often zoom in the potential region of interest (ROI) to better visualize the 3D extension and boundary of thoracic duct.

In this work, we propose a two-stage coarse-to-fine thoracic duct segmentation framework based on the anatomy prior and topology guidance. At stage one, using a recent multi-organ deep segmentation model [4], we first segment six key chest organs that are spatially related to the thoracic duct. These organ predictions are then used as anatomy guidance to better localize and segment the thoracic duct. Specifically, 3D mask image consisting six key organs is concatenated with the planning CT to serve as input to the stage one deep segmentation network. We then extract the centerline from the initial thoracic duct segmentation and use a minimum-cost path approach [9] to connect the discontinuous ones if there exists. Based on the topology-corrected centerline, CT scan and key organ mask can be resampled around the initial thoracic duct segmentation using the curved planar reformation (CPR) technique [11, 12] to generate newly reformatted 3D volumes (refer Fig. 1(c,d) as an example). The resampled CT volume provides a spatially smoother representation of thoracic duct along its medial axial direction, and used as input to the stage two segmentation network. The segmentation result of stage two is later transformed back into the original image space using inverse CPR transform. We evaluate our approach on an in-house dataset, including 117 lung cancer planning CT scans with manual thoracic duct annotations. Our approach significantly outperforms a strong baseline of nnUNet [5] by reducing 57% relative Hausdorff distance error (from 49.9mm to 21.2mm) and improving 1.8% absolute Jaccard Index.
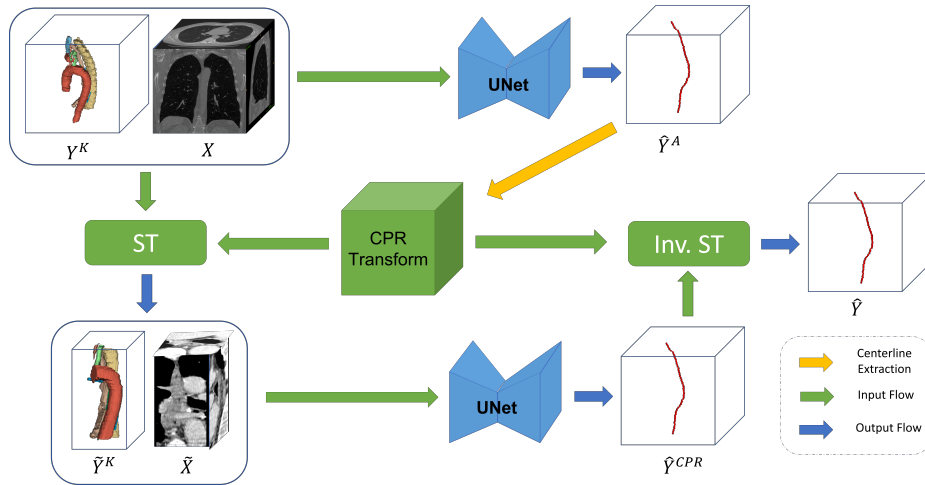
Fig. 2: Overall workflow of our proposed 2-stage Anatomy and Topology Guided Coarse-to-fine Segmentation of Thoracic Duct. ST and Inv. ST denotes Spatial Transform and Inverse Spatial Transform.

2   Methods

The proposed coarse-to-fine thoracic duct segmentation framework consists of two main stages. At stage-1, anatomy-guided coarse segmentation is conducted. At stage-2, the centerline of coarse segmentation is extracted first, which is utilized to perform the CPR transformation. After that, the fine-scale segmentation is executed in the CPR space and the segmentation output is transformed back in the original image space to get the final thoracic duct segmentation. Fig. 2 depicts an overview of our proposed method.

2.1   Anatomy-guided Coarse Segmentation

To better localize and segment thoracic duct at stage one, we first segment a set of six key organs using a recent multi-organ deep segmentation mode [4]. Six key organs include: *esophagus, aorta, spine, azygos vein, subclavian vein* and *internal jugular vein*. Their predictions are used as anatomy prior to guide the thoracic duct segmentation. Let a dataset of N instances denoted as $\mathbf{D} = \{X_n, Y_n^S, Y_n\}^N$, where X_n, Y_n^S, Y_n denote the input CT image, prediction mask of six supporting organs and ground truth mask of thoracic duct. Dropping n for clarity, the anatomy-guided segmentation model at stage one predicts a coarse thoracic duct Y^C given X and Y^S:

$$\hat{Y}^C = f^C(X, Y^S | \mathbf{W}^C) \tag{1}$$

where $f^{(*)}(.)$ and $\mathbf{W}^{(*)}$ denote the network function and the corresponding network parameters, respectively, and $\hat{Y}^C$ represents the predicted coarse thoracic

duct output. As demonstrated in the experiment, using six supporting organs leads to more accurate segmentation results with less false positives.

2.2   Segmentation Refinement through Topology-guided CPR

Although the prediction $\hat{Y}^C$ achieves overall reasonable segmentation results, however, discontinuous segmentation along vertical axis and inaccurate boundary in xy-planes may still exist. We aim to solve these issues at stage two by refining the segmentation.

It is noticed that physicians often use the curved planar reformation (CPR) to visualize vascular abnormalities for small vessels [11, 12], where CPR can generate longitudinal cross-sections of a tubular structure in a curved plane. Inspired by that, we apply the CPR to transform the planning CT into a new 3D volume representation that provides a spatially smoother reformation of thoracic duct in its elongated medial axis direction. Then, the CPR-transformed CT along with CPR-transformed organ mask are employed as input to the second stage deep segmentation network for fine-scale thoracic duct segmentation. This refinement stage two consists of the following steps: 1) extract a single and continuous centerline $\hat{C}$ from predicted thoracic duct $\hat{Y}^C$ mask even if $\hat{Y}^C$ has segmentation breakage; 2) compute CPR transformation map based on $\hat{C}$; 3) apply CPR transformation to CT and support organ mask and train a deep segmentation network using transformed CT and organ mask in CPR space, 4) apply inverse CPR transformation to get the final thoracic duct segmentation in original CT space. The centerline extraction and CPR transformation steps are described as follows.

Topology-corrected Centerline Extraction. To compute the CPR transformation, it first requires to extract a complete single centerline regardless of the number of components that $\hat{Y}^C$ has. To achieve that, consider $\hat{Y}^C$ has M connected components $\hat{Y}^C_m$ because of the breakage in the coarse segmentation. Centerline of each component $\hat{Y}^C_m$ can be extracted by a thinning algorithm [14], i.e., $\hat{C}_m = \mathrm{Thinning}(\hat{Y}^C_m)$. Then, the gap between components are connected by iteratively computing a minimum-cost path [9] between each two adjacent components. This leads to a complete connected centerline of the same topology as original thoracic duct. The process is illustrated in Fig. 1 (b).

CPR Transformation. The goal of CPR transformation is to make a tubular structure visible in it's entire length within one single image. In particular, we use the stretched CPR. To do this, thoracic duct centerline is required. Assume that the extracted centerline $\hat{C}$ of $\hat{Y}^C$ is a sequence of points at sub-voxel resolution. By processing all points successively, the corresponding lines-of-interest are mapped to the image. This is done by rotating the consecutive point around the current line-of-interest. The point is rotated in a way that the resulting plane is coplanar to the viewing plane. Let P_i to be the last processed point and point P_{i+1} the currently processed point of the centerline. The vector $\boldsymbol{d_i} = \boldsymbol{P_i P_{i+1}}$

and l represent the path direction at position i and the normalized direction of the line-of-interest respectively. The offset Δ_i in image space is derived as:

$$\Delta_i = \sqrt{|d_i|^2 - l \cdot d_i}. \tag{2}$$

The image position (y-coordinates) y_{i+1} of the line-of-interest related to point P_{i+1} is given by $y_{i+1} = y_i + \Delta_i$ where $y_0 = 0$. The resampling map is computed by consecutive viewing planes perpendicular to derived line-of-interest. An example of CPR transformed CT using centerline of thoracic duct is shown in Fig. 1 (c) with its grid transform map in (d).

3   Experiments and Results

Dataset. After obtaining approval by the appropriate institutional review board, we retrospectively collected patients with primary lung cancer treated by radiotherapy from May 2005 to February 2020 at The University of Hong Kong, Shenzhen Hospital. A total of 117 patients with RT planning CT were included, with an average CT volume size of $514 \times 514 \times 139$ voxels and an average voxel resolution of $1.2 \times 1.2 \times 3.0\mathrm{mm}^3$. The thoracic duct is manually delineated by an experienced radiation oncologist (10 yr) with the guidance of a second senior radiation oncologist (25 yr), while the segmentation of six supporting organs, including azygos vein, aorta, esophagus, spine, left internal jugular vein and left subclavian vein, are provided using a recent multi-organ segmentation model [4].

Implementation details. We adopt '3d-fullres' version of nnUNet [5] with Dice+CE losses as our backbone modules. Each encoder is the same as the default nnUNet encoder. We use the default nnU-Net data augmentation settings for our model training, and set the patch size to $192\times192\times48$ and $96\times96\times208$ for 1st and 2nd stages. We implemented our framework using PyTorch and trained on an NVIDIA Tesla V100. The total training epochs is 500. The average training time is 0.5 GPU days. For CPR transform, we set the field of view to 6.4×6.4 cm and adopt a resampling spacing of $0.5 \times 0.5 \times 1.5$ mm.

Comparing method and evaluation metrics. We employ five-fold cross-validation protocol split at the patient level. As there is no previous works solving the thoracic duct segmentation, we compare our method with nnUNet [5], which represents the current leading organ segmentation approach and use it as our segmentation backbone. Three quantitative metrics are reported to evaluate the thoracic duct segmentation performance: Jaccard Index (Jac.), Dice score (DSC), and Hausdorff distance (HD) in "mm". We further divide the whole thoracic duct (TD) into two anatomical segments, upper TD and lower TD based on the top of aortic arch, and report their corresponding quantitative metrics, respectively.

Quantitative results.

Table 1: Quantitative ablation results for proposed 2-stage Thoracic Duct (TD) segmentation framework using nnUNet [5] as backbone. AG represents the anatomy-guided coarse segmentation (with six key supporting organs). CPR refers to the topology-guided curved planar reformation based segmentation. DSC and Jacarrd (Jac.) Index are shown in "%" and Hausdorff distance (HD) in "mm".

AG	CPR	Upper TD			Lower TD			Whole TD		
		Jac.	DSC	HD	Jac.	DSC	HD	Jac.	DSC	HD
−	−	21.31	32.85	34.89	47.45	63.96	29.71	42.48	59.18	49.79
✓	−	27.88	41.90	28.32	47.67	64.17	20.58	43.24	60.04	38.19
−	✓	26.78	41.70	28.11	47.38	63.68	27.56	43.27	58.06	40.44
✓	✓	**30.21**	**43.99**	**12.22**	**48.87**	**65.34**	**14.46**	**44.15**	**60.09**	**21.18**

Our quantitative ablation results which demonstrate the effectiveness of each component in the proposed framework and comparison to leading general organ segmentation approach nnUNet [5] are tabulated in Table 1. The volumetric index of Jac. or DSC scores are low in general. This indicates the difficulty of this task. However, we can observed that by applying the proposed anatomy guidance using six key support organs to nnUNet newtork (row 2 vs. row 1), HD drops from 49.79 mm to 38.19 mm, meanwhile improves the absolute Jac. score by 0.8%. Especially, for upper TD region, the Dice score increase around 30%, from 32.85% to 41.90% which clearly demonstrated the importance of incorporating anatomy priors for segmenting small and hard organs in CT scans. The effectiveness of proposed topology-guided CPR based segmentation refinement is first validated by comparing row 3 vs. row 1 where one can observe a similar improvement as using anatomy guidance. Note that, since our proposed framework is a two-stage pipeline, the performance of stage 2 relies on the output of stage 1. Thus, although the AG or CPR alone can help better segment the thoracic duct, their combination further significantly improves the results (row 4 vs. row 2/3). For instance, even if AG is already utilized in the nnUNet model to guide the segmentation, combining it with the second stage CPR segmentation refinement still leads to an additional 16 mm, 6 mm and 17 mm Hausdorff distance error reduction in upper, lower and whole TD respectively. When compared with original nnUNet, our complete 2-stage framework (AG + CPR) showed a significant improvement in terms of all metrics (row 4 vs. row 1). Furthermore, we examined the inter-observer variation in 117 patients. The consistency between two physicians following our internal delineation guideline is 64.64% in Dice score. As comparison, our method achieves 60.09% Dice score.

Qualitative results. Apart from the quantitative comparison, we also compare our method with nnUNet qualitatively by the visual inspection. Three qualitative results are shown in Fig. 3. As can be observed, the proposed 2-stage method can generate topology desired and more complete thoracic duct segmentation. In contrast, nnUNet yields several clear segmentation breakages. While our stage one segmentation model (nnUNet with AG) can reasonably improve the performance, breakages or under-segmentations still exist as shown in the figure. With

CT	**Ground Truth**	**nnUNet**	**AG**	**AG+CPR**
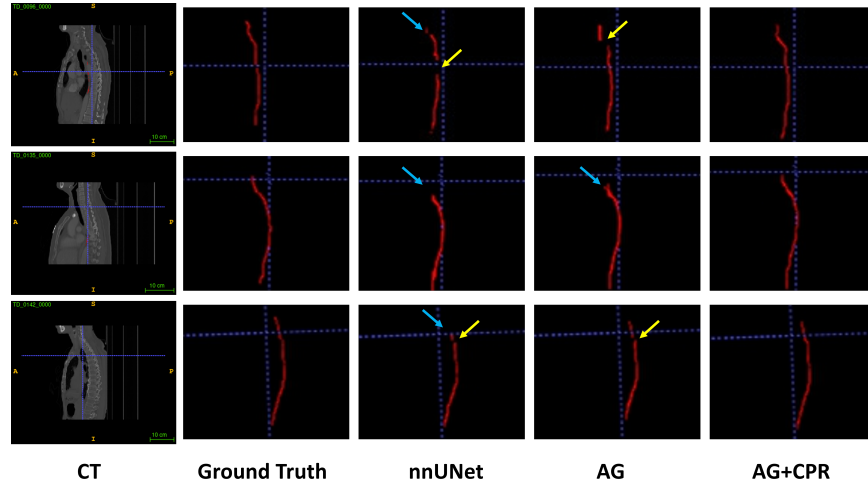
Fig. 3: Qualitative results of thoracic duct segmentation in three patients using different methods. nnUNet is the leading comparison method. AG is our stage one segmentation method, while AG+CPR represents the proposed two-stage method. Segmentation breakages and missing thoracic duct are indicted by yellow and blue arrows, respectively.

AG+CPR as our proposed 2 stage framework, all previous defects are absent in all three example cases.

4   Conclusion

In this work, we present a two stage coarse-to-fine thoracic duct segmentation approach. Recent studies have emphasized the importance of protecting thoracic duct during radiation therapy, and we are the first to tackle this clinically critical yet under-studied task using an automated method. Because of its thin/slim size, curved geometry and extremely poor (intensity) contrast of thoracic duct, we propose to use anatomy priors and topology guidance in a two stage framework to address these challenges. At stage one, six key chest organs are automatically segmented and combined with the planning CT to better infer and localize the thoracic duct. At stage two, we subsequently extract the centerline of initial thoracic duct segmentation, where curved planar reformation is applied to transform the planning CT into a new 3D volume representation that provides a spatially smoother reformation of thoracic duct in its elongated medial axis direction. Then, the CPR-transformed CT is employed as input to the stage two deep segmentation network, and the output prediction is transformed back to the original image space, as the final thoracic duct segmentation. Experimental results demonstrate the effectiveness of our approach, as it significantly outperforms a strong baseline nnUNet by reducing 57% relative HD error (from 49.9mm to 21.2mm) and improving 1.8% absolute Jaccard Index.

Bibliography

[1] Chen, X., Sun, S., Bai, N., Han, K., Liu, Q., Yao, S., Tang, H., Zhang, C., Lu, Z., Huang, Q., et al.: A deep learning-based auto-segmentation system for organs-at-risk on whole-body computed tomography images for radiation therapy. Radiotherapy and Oncology **160**, 175–184 (2021)

[2] Davuluri, R., Jiang, W., Fang, P., Xu, C., Komaki, R., Hsu, C., et al.: Absolute lymphocyte count nadir during chemoradiation as a prognostic indicator of esophageal cancer survival outcomes. International Journal of Radiation Oncology, Biology, Physics **96**(2), E177 (2016)

[3] Guo, D., Jin, D., Zhu, Z., Ho, T.Y., Harrison, A.P., Chao, C.H., Xiao, J., Lu, L.: Organ at risk segmentation for head and neck cancer using stratified learning and neural architecture search. In: IEEE/CVF Conference on Computer Vision and Pattern Recognition. pp. 4223–4232 (2020)

[4] Guo, D., Ye, X., Ge, J., Di, X., Lu, L., Huang, L., Xie, G., Xiao, J., Lu, Z., Peng, L., et al.: Deepstationing: thoracic lymph node station parsing in ct scans using anatomical context encoding and key organ auto-search. In: MICCAI. pp. 3–12. Springer (2021)

[5] Isensee, F., Jaeger, P.F., Kohl, S.A., Petersen, J., Maier-Hein, K.H.: nnu-net: a self-configuring method for deep learning-based biomedical image segmentation. Nature methods **18**(2), 203–211 (2021)

[6] Ji, Z., Guo, D., Wang, P., Yan, K., Ge, J., Ye, X., Xu, M., Zhou, J., Lu, L., Gao, M., et al.: Continual segment: Towards a single, unified and accessible continual segmentation model of 143 whole-body organs in ct scans. In: IEEE International Conference on Computer Vision (2023)

[7] Jin, D., Guo, D., Ge, J., Ye, X., Lu, L.: Towards automated organs at risk and target volumes contouring: Defining precision radiation therapy in the modern era. Journal of the National Cancer Center (2022)

[8] Jin, D., Guo, D., Ho, T.Y., Harrison, A.P., Xiao, J., Tseng, C.K., Lu, L.: Deeptarget: Gross tumor and clinical target volume segmentation in esophageal cancer radiotherapy. Medical Image Analysis **68**, 101909 (2021)

[9] Jin, D., Iyer, K.S., Chen, C., Hoffman, E.A., Saha, P.K.: A robust and efficient curve skeletonization algorithm for tree-like objects using minimum cost paths. Pattern recognition letters **76**, 32–40 (2016)

[10] Jin, J.Y., Mereniuk, T., Yalamanchali, A., Wang, W., Machtay, M., Ellsworth, S., et al.: A framework for modeling radiation induced lymphopenia in radiotherapy. Radiotherapy and Oncology **144**, 105–113 (2020)

[11] Kanitsar, A., Fleischmann, D., Wegenkittl, R., Felkel, P., Groller, E.: CPR-curved planar reformation. IEEE (2002)

[12] Kanitsar, A., Wegenkittl, R., Fleischmann, D., Groller, M.E.: Advanced curved planar reformation: Flattening of vascular structures. IEEE (2003)

[13] Kiyonaga, M., Mori, H., Matsumoto, S., Yamada, Y., Sai, M., Okada, F.: Thoracic duct and cisterna chyli: evaluation with multidetector row ct. The British journal of radiology **85**(1016), 1052–1058 (2012)

[14] Lee, T.C., Kashyap, R.L., Chu, C.N.: Building skeleton models via 3-d medial surface axis thinning algorithms. CVGIP: graphical models and image processing **56**(6), 462–478 (1994)

[15] Liu, J., Yang, L., Zhang, J., Wang, Q., Jiang, X., Qing, G., Kong, F.: Integrate sequence information of dose volume histogram in training lstm-based deep learning model for lymphopenia diagnosis. International Journal of Radiation Oncology, Biology, Physics **111**(3), e112–e113 (2021)

[16] Schnyder, P., Hauser, H., Moss, A., Gamsu, G., Brasch, R., Bohnet, J., Candardjis, G.: Ct of the thoracic duct. European Journal of Radiology **3**(1), 18–23 (1983)

[17] Shi, F., Hu, W., Wu, J., Han, M., Wang, J., Zhang, W., Zhou, Q., Zhou, J., Wei, Y., Shao, Y., et al.: Deep learning empowered volume delineation of whole-body organs-at-risk for accelerated radiotherapy. Nature Communications **13**(1), 6566 (2022)

[18] Siegel, R.L., Miller, K.D., Fuchs, H.E., Jemal, A.: Cancer statistics, 2022. CA: A Cancer Journal for Clinicians **72**(1), 7–33 (2022)

[19] So, T.H., Chan, S.K., Chan, W.L., Choi, H., Chiang, C.L., Lee, V., et al.: Lymphopenia and radiation dose to circulating lymphocytes with neoadjuvant chemoradiation in esophageal squamous cell carcinoma. Advances in Radiation Oncology **5**(5), 880–888 (2020)

[20] Tang, C., Liao, Z., Gomez, D., Levy, L., Zhuang, Y., Gebremichael, R.A., et al.: Lymphopenia association with gross tumor volume and lung v5 and its effects on non-small cell lung cancer patient outcomes. International Journal of Radiation Oncology* Biology* Physics **89**(5), 1084–1091 (2014)

[21] Tang, H., Chen, X., Liu, Y., Lu, Z., You, J., Yang, M., et al.: Clinically applicable deep learning framework for organs at risk delineation in ct images. Nature Machine Intelligence **1**(10), 480–491 (2019)

[22] Tyldesley, S., Boyd, C., Schulze, K., Walker, H., Mackillop, W.J.: Estimating the need for radiotherapy for lung cancer: an evidence-based, epidemiologic approach. International Journal of Radiation Oncology* Biology* Physics **49**(4), 973–985 (2001)

[23] Wang, P., Guo, D., Zheng, D., Zhang, M., Yu, H., Sun, X., Ge, J., Gu, Y., Lu, L., Ye, X., et al.: Accurate airway tree segmentation in ct scans via anatomy-aware multi-class segmentation and topology-guided iterative learning. arXiv preprint arXiv:2306.09116 (2023)

[24] Xu, C., Jin, J.Y., Zhang, M., Liu, A., Wang, J., Mohan, R., Lin, S.H., et al.: The impact of the effective dose to immune cells on lymphopenia and survival of esophageal cancer after chemoradiotherapy. Radiotherapy and Oncology **146**, 180–186 (2020)

[25] Ye, X., Guo, D., Ge, J., Yan, S., Xin, Y., Song, Y., Yan, Y., Huang, B.S., Hung, T.M., Zhu, Z., et al.: Comprehensive and clinically accurate head and neck cancer organs-at-risk delineation on a multi-institutional study. Nature Communications **13**(1), 6137 (2022)

[26] Zhu, Z., Jin, D., Yan, K., Ho, T.Y., Ye, X., Guo, D., Chao, C.H., Xiao, J., Yuille, A., Lu, L.: Lymph node gross tumor volume detection and segmentation via distance-based gating using 3d ct/pet imaging in radiotherapy. In: MICCAI. pp. 753–762. Springer (2020)